

Effects of lateral modes on the static and dynamic behaviour of buried heterostructure DFB lasers

S.F. Yu
E.H. Li

Indexing terms: Lasers, Lateral modes, Semiconductor laser diodes, Transient response

Abstract: The transient response of buried-heterostructure distributed-feedback laser is studied. It is found that the gain margin between the lateral modes is affected by the carrier-diffusion length in the active region. In addition, the transient response of the lateral modes is also influenced by the carrier-diffusion length.

1 Introduction

High-power single-mode single-element lasers with fast response are required for wavelength-sensitive applications such as frequency doubling, atomic spectroscopy or pumping sources. The ideal devices for these applications are the buried-heterostructure (BH), distributed-feedback (DFB) and distributed-Bragg-reflector (DBR) semiconductor-laser diodes [1, 2] because these devices can operate at high power, with a single and stable longitudinal mode [3, 4] as well as exhibiting low threshold current and high operation temperature [5].

The maximum output power of laser diodes is affected by the width of the active region [4]. The maximum optical power is increased with the width of active region but this will cause the excitation of high-order lateral modes. In the design of high-power lasers, either stable lateral modes are allowed to lase or single mode operation is maintained to a maximum output power [4, 6]. In both cases, high-order lateral modes are supported by the waveguide and can be excited by an electrical signal with large amplitude. Therefore, a different design strategy is required to improve the gain margin between the lateral modes and without reducing the width of the active region.

It has been shown that lateral effects can significantly affect the dynamic behaviour of DFB lasers [7]. However, in our previous analysis only the fundamental mode was considered in the calculation. In fact, the standing-wave patterns of the lateral modes are very different, as are the carrier distributions (in lateral and longitudinal directions). Therefore, the dynamic and static responses of DFB lasers can be modified significantly by the lateral modes.

In this paper, the transient responses of the devices are analysed including the effects of lateral modes. Further, the influence of the lateral and longitudinal carrier dis-

tribution on the gain margin (between the lateral modes) is studied. A new large-signal dynamic model of DFB lasers including lateral modes is also developed for these purposes. This model also takes into account the two-dimensional (longitudinal and lateral) variations of carrier density, photon density and refractive index.

2 Laser structure

The laser structure used in our analysis is the BH InGaAs/GaAs (0.98 μm) separate-confinement/single-quantum-well (SCH-SQW) DFB laser [1] with second-order grating. A schematic of the device is shown in Fig. 1. The laser is composed of seven layers, the p^+ -GaAs

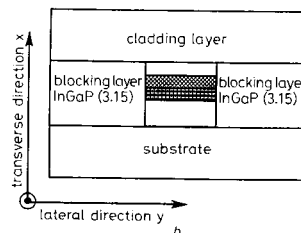
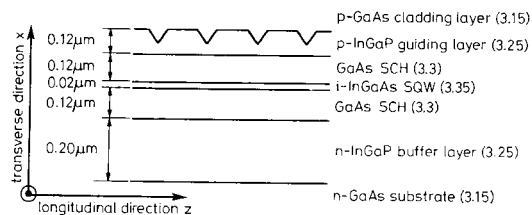


Fig. 1 Schematic of buried-heterostructure separate-confinement single-quantum well distributed feedback laser

a Side view of DFB laser
b Cross-section of the DFB laser
Dimensions in μm

cladding layer, the p -InGaP guiding layer, the InGaAs-GaAs SCH-SQW active region, the n -InGaP buffer layer and n^+ -GaAs substrate. The current-blocking layers are

The work is supported by the HKU-CRCG grants. The authors thank M.C. Nowell for the supply of laser parameters used in the calculation, and one of the referees for comments on the paper.

© IEE, 1995

Paper 1855J (E13), first received 8th September 1994 and in revised form 3rd January 1995

The authors are with the University of Hong Kong, Department of Electrical & Electronic Engineering, Pokfulam Road, Hong Kong

of InGaP material. Using the parameters given in Fig. 1, it can be shown that only the fundamental transverse mode is supported along the transverse direction. In addition, for the width of active region greater than 1.0 μm , the first-order lateral mode can also be supported by the waveguide.

3 Laser model

The laser model used to analyse the lateral modes of the DFB laser is an extension of that in Reference 7. The time-dependent coupled-wave equations for the forward and reverse fields F and R are given as

$$\left(\frac{1}{v_g} \frac{\partial}{\partial t} + \frac{\partial}{\partial z}\right) F_j = (g_j + i\delta\beta_j - \alpha_{sj} - h_{1j}) F_j + i(\kappa_j + ih_{1j}) R_j \quad (1)$$

$$\left(\frac{1}{v_g} \frac{\partial}{\partial t} - \frac{\partial}{\partial z}\right) R_j = (g_j + i\delta\beta_j - \alpha_{sj} - h_{1j}) R_j + i(\kappa_j + ih_{1j}) F_j \quad (2)$$

where j is the lateral mode number. In eqns. 1 and 2, it is assumed that the j th lateral mode has a set of longitudinal (DFB) modes [8]. κ_j is the coupling coefficient and h_{1j} is radiation loss coefficient of the j th mode. g_j is the field gain of the j th lateral mode and is given by

$$g_j(z, t) = \int_{\text{active}} \frac{\Gamma_x g_N \{N(y, z, t) - N_0\} \psi_j^2(y, z, t)}{2(1 + \varepsilon P)} dy \quad (3)$$

where N is the carrier distribution in the lateral and longitudinal directions, Γ_x is the transverse confinement factor, g_N is the differential gain, ε is the gain-compression coefficient and P is the photon density. The total absorption and scattering losses α_{sj} of the j th mode are given by

$$\alpha_{sj} = \alpha_a \int_{\text{active}} \psi_j^2(y, z, t) dy + \alpha_b \left\{ 1 - \int_{\text{active}} \psi_j^2(y, z, t) dy \right\} \quad (4)$$

where α_a is the absorption and scattering loss inside the optical-confinement region and α_b is the free-carrier absorption-loss coefficient associated with the blocking layer. If lateral effects are not considered in this model, the discrimination of lateral modes is only determined by eqn. 4.

$\delta\beta_j (= \beta_j - \beta_0)$ is the deviation from Bragg frequency ($\beta_0 = 2\pi/\Lambda_0$), where β_j is the propagation coefficient of the j th lateral mode and Λ_0 is the grating period. The lateral field ψ_j , the propagation coefficient β_j and the equivalent longitudinal effective index n_{effj} can be deduced from the wave equation

$$\left\{ \frac{\partial^2}{\partial y^2} + k_0^2 \varepsilon_{eff}(y, z, t) \right\} \psi_j(y, z, t) = \beta_j^2(z, t) \psi_j(y, z, t) \quad (5)$$

ε_{eff} in eqn. 5 is the effective permittivity and is given by

$$\begin{aligned} \varepsilon_{eff}(y, z, t) &= n_{effa}^2(y) - n_{effa}(y) \Gamma_x \frac{\alpha_m \lambda_0}{2\pi} g_N \{N(y, z, t) - N_{th}\} \\ &\quad + i \frac{n_{effa}(y)}{k_0} \Gamma_x [g_N \{N(y, z, t) - N_0\} - \alpha(y)] \end{aligned} \quad (6)$$

where n_{effa} is the effective (build-in) refractive index of the waveguide region, α_m is the material linewidth-enhancement factor, $k_0 (= 2\pi/\lambda_0)$ is the wavenumber and

N_{th} is the threshold carrier concentration. $\alpha(y) = \alpha_a$ inside the active region and $\alpha(y) = \alpha_b$ elsewhere. The equivalent effective index n_{effj} is defined as

$$n_{effj}(z, t) = \frac{\beta_j(z, t)}{k_0} \quad (7)$$

The time-dependent rate equation of carrier concentration is given by

$$\begin{aligned} \frac{dN(y, z, t)}{dt} &= \frac{J(z, t)}{qd} - \frac{N(y, z, t)}{\tau} - v_g \frac{g_N \{N(y, z, t) - N_0\}}{(1 + \varepsilon P)} \\ &\quad \times P(y, z, t) + D \nabla^2 N(y, z, t) \end{aligned} \quad (8)$$

where d is the thickness of the active layer, D is the diffusion constant, τ is the carrier lifetime, q is the electron charge and J is the injection current-density profile. It is assumed that J is uniform in the lateral direction. The photon density P is given as

$$\begin{aligned} P(y, z, t) &= \{ |F_j(z, t)|^2 + |R_j(z, t)|^2 \} \psi_j^2(y, z, t) \\ &= P_j(z, t) \psi_j^2(y, z, t) \end{aligned} \quad (9)$$

The inhomogeneous distribution of carriers in the lateral direction is caused by the standing-wave pattern of the intensity of the lateral modes, as well as by the carrier diffusion length. Fig. 2 shows the intensity distribution of

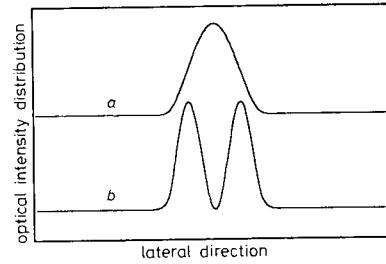


Fig. 2 Optical intensity distribution of fundamental and first-order lateral modes

a Fundamental mode
b First-order mode

the fundamental and the first-order modes. Thus the carrier distribution in the lateral direction can be approximated by [9]

$$N(y, z, t) = N_p(z, t) + \sum_{k=1} (-1)^k N_k(z, t) \cos(2k\pi y/w) \quad (10)$$

where w is the width of the active region. The coefficients N_p, N_1, N_2, \dots are, respectively, the Fourier coefficients representing the amplitudes of the various components used in the description of the inhomogeneous distribution of carrier. The simplified field gain $g_j(z, t)$ can be obtained by substituting eqn. 10 into eqn. 3, which gives

$$g_j = \frac{\Gamma_x g_N \left\{ \Gamma_y f(N_p - N_0) + \sum_{k=1} (-1)^k \xi_{k,j} N_k \right\}}{2(1 + \varepsilon P)} \quad (11)$$

where $k = 1, 2, 3, \dots$. The space-independent (in lateral-direction) rate equations can be obtained from eqns. 8 and 10 and are

$$\begin{aligned} \frac{dN_p}{dt} &= \frac{J}{qd} - \frac{N_p}{\tau} \\ &\quad - v_g g_N \sum_j \frac{\left\{ \Gamma_y f(N_p - N_0) + \sum_{k=1} (-1)^k \xi_{k,j} N_k \right\} P_j}{1 + \varepsilon P} \end{aligned} \quad (12)$$

$$\frac{dN_k}{dt} = \frac{(-1)^{k+1} 2v_g g_N}{1 + \varepsilon P} \times \sum_j \left\{ \zeta_{k,j} (N_p - N_0) + \sum_{m=1} (-1)^m \chi_{k,m,j} N_m \right\} P_j - \frac{1 + \gamma_k}{\tau} N_k \quad (13)$$

where $m = 1, 2, 3, \dots$, and

$$\begin{aligned} \gamma_k &= \left(\frac{2k\pi L_{eff}}{w} \right)^2 \\ \Gamma_{y,j} &= \int_{-w/2}^{w/2} \psi_j^2(y, z, y) dy \\ \zeta_{k,j} &= \int_{-w/2}^{w/2} \cos(2k\pi y/w) \psi_j^2(y, z, t) dy \\ \chi_{k,m,j} &= \int_{-w/2}^{w/2} \cos(2k\pi y/w) \cos(2m\pi y/w) \psi_j^2(y, z, t) dy \end{aligned} \quad (14)$$

where L_{eff} is the effective diffusion length and is defined as $L_{eff} = \sqrt{D\tau}$.

A space-consistent large-signal calculation can be obtained by solving eqns. 1, 2, 12 and 13 simultaneously [10]. In the model, the longitudinal variation of carrier density and field intensity are taken into account by dividing the laser cavity into a number of small equal sections. In each section, the nonuniform distribution of lateral field and carrier profile are determined by eqns. 5 and 10.

In a strong guiding device, the variation of the lateral field ψ_j and the propagation coefficient β_j caused by the external carrier injection may be less than 10%. The small variation of lateral field $\Delta\psi_j$ and propagation coefficient, $\Delta\beta_j$ can be estimated by a first-order perturbation method [11]. The wave equation (eqn. 5), can be rewritten as

$$\left\{ \frac{\partial^2}{\partial y^2} + \varepsilon_{eff,s}(y, z) k_0^2 \right\} + \Delta\varepsilon_{eff}(y, z, t) k_0^2 \psi_f(y, z, t) = \beta_j^2(z, t) \psi_f(y, z, t) \quad (15)$$

where $\psi_j = \psi_{js} + \Delta\psi_j$ and $\beta_j = \beta_{js} + \Delta\beta_j$. The subscript s stands for the unperturbed values. The approximated solutions for $\Delta\beta_j$ and $\Delta\psi_j$ are given as [11]

$$\left. \begin{aligned} \Delta\beta_j(z, t) &= \frac{k_0^2 \int \psi_{js}^*(y, z) \Delta\varepsilon(y, z, t) \psi_{js}(y, z) dy}{2\beta_{js}(z) \int |\psi_{js}(y, z)|^2 dy} \\ \Delta\psi_f(y, z, t) &= \frac{1}{\int |\psi_{js}(y, z)|^2 dy} \\ &\quad \times \sum_{j \neq n} \frac{k_0^2 \int \psi_{ns}^*(y, z) \Delta\varepsilon(y, z, t) \psi_{js}(y, z) dy}{\{\beta_{js}^2(z) - \beta_{ns}^2(z)\}} \\ &\quad \times \psi_{ns}(y, z) \end{aligned} \right\} \quad (16)$$

where n is the lateral-mode number.

4 Parameters

It is assumed that the differential gain and the linewidth-enhancement factor of the SQW are $2.4 \times 10^{-15} \text{ cm}^2$ and 3.0, respectively. The length of the laser is $400 \mu\text{m}$ and the width of the active region is $2 \mu\text{m}$. The thickness of the SQW is $0.02 \mu\text{m}$. The confinement factor Γ_x in the transverse direction is found to be equal to 0.0462. The coupling coefficient κ and the radiation-loss coefficient h_1 of the fundamental and first-order modes are approximately equal to 50 and 7.0 cm^{-1} , respectively. The absorption and scattering losses α_a and α_s are assumed to be equal to 20.0 cm^{-1} . The nonlinear gain coefficient ε is set to $2 \times 10^{-17} \text{ cm}^3$. The other device parameters used in the model can be found in Table 1. In the following calculations, only the fundamental and first-order lateral modes are considered.

Table 1: Parameters used in the model

Carrier lifetime τ	$3 \times 10^{-9} \text{ s}$
Differential gain g_N	$2.4 \times 10^{-15} \text{ cm}^2$
Transparency carrier density N_0	$1.0 \times 10^{18} \text{ cm}^{-3}$
Linewidth-enhancement factor α_m	3.0
Absorption and scattering loss (energy) in waveguide α_a	20 cm^{-1}
Free-carrier absorption loss in blocking layer α_b	20 cm^{-1}
Effective group refractive index n_g	3.70
Length of the laser cavity L	$400 \mu\text{m}$
Width of active region w	$2.0 \mu\text{m}$
Thickness of the active layer d	$0.02 \mu\text{m}$
Approximate emission wavelength λ_0	$0.98 \mu\text{m}$
Period of grating Λ_0	$0.3 \mu\text{m}$
Nonlinear gain-suppression coefficient ε	$2 \times 10^{-17} \text{ cm}^3$
Transverse confinement factor Γ_x	0.0462
Coupling coefficient $\kappa_0 \cong \kappa_1$	50.0 cm^{-1}
Radiation-loss coefficient ($h_{10} \cong h_{11}$)	7.0 cm^{-1}

5 Simulation results

The device under investigation is a $\lambda/4$ phase-shifted DFB structure with both facets antireflection (AR) coated. The laser is initially biased at threshold and then modulated with a step current. The steady-state optical power from the AR facets is kept below 11 mW such that the power level of side modes (cavity modes) is negligible and can be ignored in our calculation.

Fig. 3 shows the switch-on transient response of the lateral modes with variation of the normalised carrier-diffusion length. In Fig. 3a, the normalised carrier-diffusion length L_{eff}/w is set to 0.4. The device shows lateral-mode competition. It is observed that both modes come up initially, but the first-order lateral mode suppresses the second overshoot (time 'o2') of the fundamental mode. Eventually, the first-order mode comes up with the fundamental mode. However, for L_{eff}/w equal or larger than 4.0, the first-order mode is quickly suppressed after the first overshoot (time 'o1') of the modes. This is shown in Fig. 3b and c.

The transient response of the lateral modes can be explained by the coupling efficiency between the lateral gain distribution and the optical-field profile [12], and the effective carrier lifetime $\tau_{eff} = L_{eff}^2/D$ in the active region.

(a) $L_{eff}/w = 0.4$ (i.e. $\tau_{eff} < 0.1 \text{ ns}$) (Fig. 4)

At time 'o1', the fundamental mode causes a high stimulated recombination rate at the centre of the waveguide and burns a hole in the lateral carrier profile. This reduces the coupling efficiency between the gain profile and the fundamental mode and reduces the gain margin

between the lateral modes. As a result, N_2 increases to a large value of $1 \times 10^{17} \text{ cm}^{-3}$.

At time 'u1' (first undershoot of optical power), the magnitude of N_1 remains high. In addition, the magni-

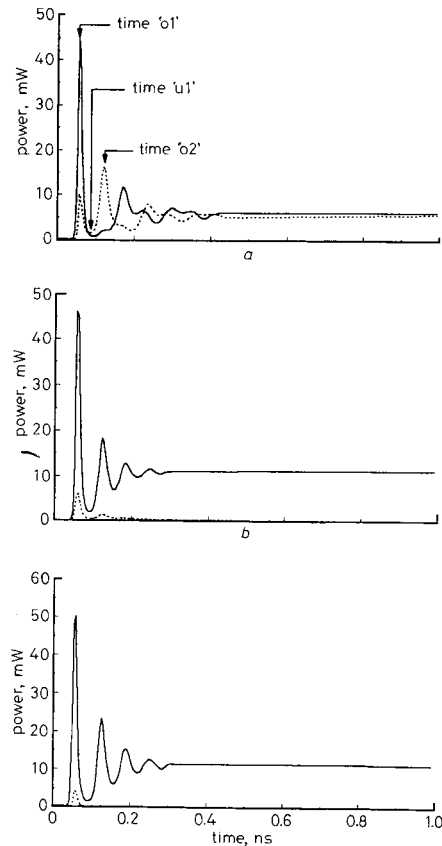


Fig. 3 Transient response of fundamental (solid line) and first-order lateral modes (broken line) under direct modulation of step current

- a $L_{eff}/w = 0.4$
- b $L_{eff}/w = 4.0$
- c $L_{eff}/w = 10$

tude of N_2 increase rapidly to its maximum value. These are caused by the short carrier lifetime (the carriers disappear rapidly before they can diffuse and smooth out the SHB). The strength of the SHB resulting from both modes is of the same order of magnitude. Notice that the strength of the SHB resulting from the fundamental mode is indicated by the magnitude of N_1 . This is also true for the first-order mode and N_2 .

At time 'o2', the first-order mode is excited (see Fig. 3a). This is because the change in N_2 during the time interval between 'u1' and 'o2' is of same order of magnitude of N_1 . Fig. 6a shows the steady-state carrier distribution of N_1 and N_2 . The diagram shows that the optical intensity of both modes depletes the active region significantly.

(b) $L_{eff}/w = 4.0$ (i.e. $\tau_{eff} > 0.1 \text{ ns}$) (Fig. 5)

At time 'o1', the magnitude of N_1 (average value is $0.3 \times 10^{17} \text{ cm}^{-3}$) is less than for $L_{eff}/w = 0.4$ (average value is $1.0 \times 10^{17} \text{ cm}^{-3}$). In addition, at time 'u1', the magnitude of N_1 is reduced to a value lower than its

peak value. This is caused by the long effective carrier lifetime, and the gain margin between the lateral modes remains at a satisfactory value. Therefore, the first-order

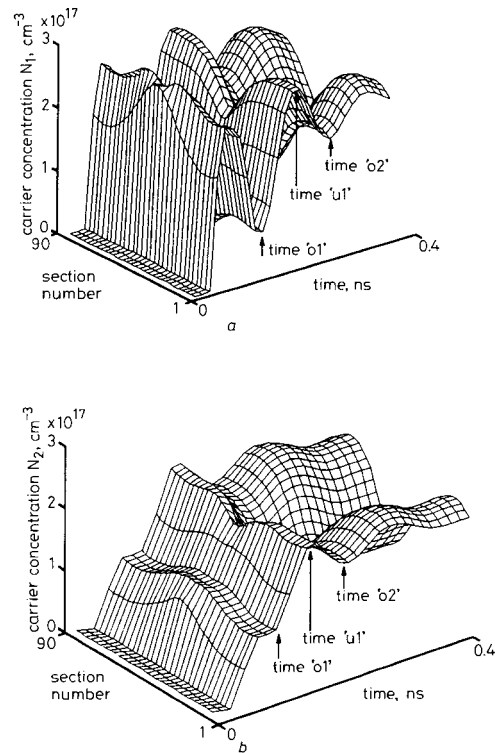


Fig. 4 Transient response of carrier distribution

- a N_1 under direct modulation of step current
 - b N_2 under direct modulation of step current
- Normalised carrier-diffusion length $L_{eff}/w = 0.4$

mode is suppressed (see Fig. 3b) at and after time 'o2'. It is also observed that N_2 has a value one-tenth of that shown in Fig. 4.

In the above discussion of lateral-modes competition, the effect of longitudinal carrier distribution has not been taken into consideration. In fact, N_1 and N_2 are strongly connected with the longitudinal field profile and carrier distribution. The longitudinal and lateral carrier distributions are coupled together by eqn. 8. The nonuniform distribution of N_1 and N_2 along the laser cavity will affect the longitudinal distribution of n_{eff} through eqn. 7. As a result, the resonant conditions of the cavity modes will be altered. This is shown in Fig. 6. For $L_{eff}/w = 0.4$, the first-order mode is excited and the distribution of N_2 shown a concave profile. However for $L_{eff}/w = 4.0$, a convex profile of N_2 is observed and the first-order mode is suppressed.

The above calculation procedures are repeated for an uniform grating DFB laser with both facets AR coated. It is found that the uniform-grating DFB laser has similar static and dynamic characteristics to those of the $\lambda/4$ device, i.e. for short L_{eff} the first-order mode is excited, but for long L_{eff} , the first-order mode is suppressed. In addition, the steady-state carrier profile of N_2 is also concave for short L_{eff} and convex for long L_{eff} (see Fig. 7). We believed this to be a main characteristic of DFB lasers.

The average gain margin $\langle \Delta g \rangle$ between the fundamental and lateral modes is also plotted against the normalised carrier-diffusion length and is shown in Fig. 8. The

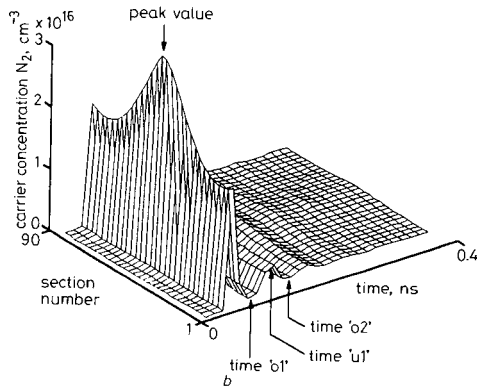
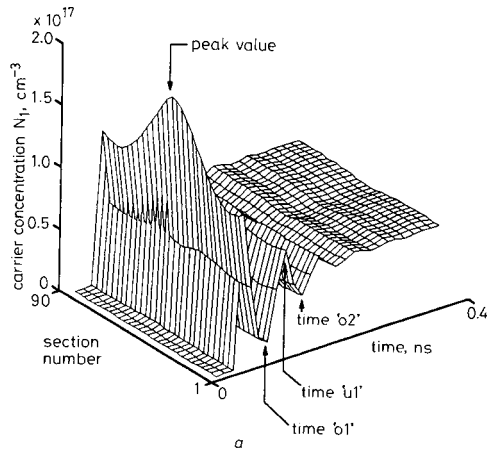


Fig. 5 Transient response of carrier distribution

a N_1 under direct modulation of step current
b N_2 under direct modulation of step current
Normalised carrier-diffusion length $L_{eff}/w = 4.0$

average gain margin can be calculated from eqn. 11 and is given by

$$\langle \Delta g \rangle = 2(\langle g_0 \rangle - \langle g_1 \rangle) \quad (17)$$

where $\langle \rangle$ is the average along the longitudinal direction. In the calculations, the steady-state optical power of the devices are biased around 10 mW.

A kink is observed for L_{eff}/w around 3. This is the point that the first-order mode starts to be suppressed by the lateral effects. It is also shown that the gain margin between the lateral modes can be improved by more than 3.0 cm^{-1} . The gain margin is determined not only by the effective lifetime of the carriers, but other laser parameters such as differential gain, internal loss and the coupling coefficient of the laser will also shift the position of the kink.

6 Discussion and conclusions

From the analysis given in Section 5, it is shown that the gain margin between the fundamental and first-order

mode can be improved by increasing the effective carrier lifetime inside the active region. Although the effective carrier lifetime is the intrinsic property of the bulk

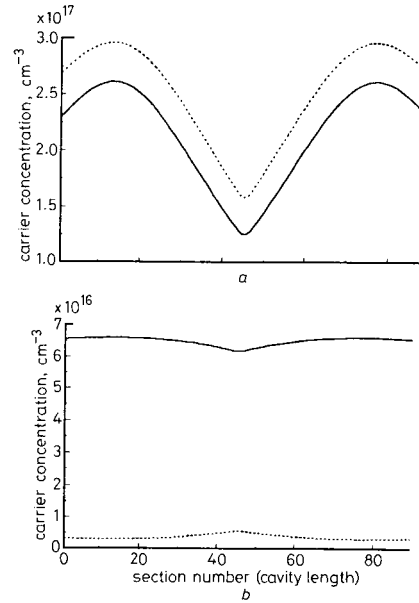


Fig. 6 Steady-state carrier distribution of N_1 (solid line) and N_2 (dotted line) for $\lambda/4$ phase-shifted DFB laser with facets antireflection coated

a Normalised carrier-diffusion length $L_{eff}/w = 0.4$
b $L_{eff}/w = 4.0$

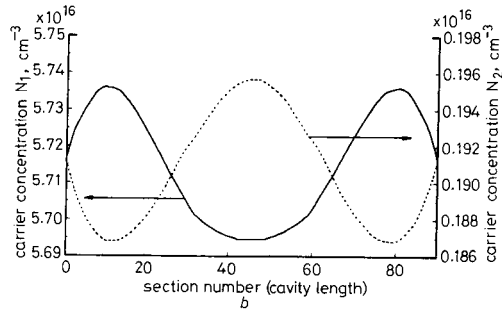
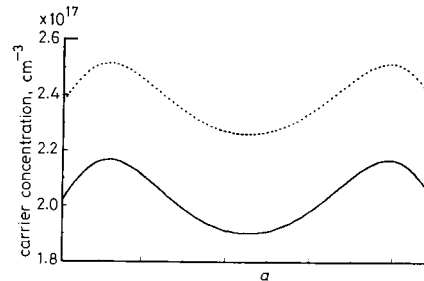


Fig. 7 Steady-state carrier distribution of N_1 (solid line) and N_2 (dotted line) for uniform-grating DFB laser with facets antireflection coated

a Normalised carrier-diffusion length $L_{eff}/w = 0.4$
b $L_{eff}/w = 4.0$

material, QW materials with different confinement structures can exhibit different effective carrier lifetimes. The effective carrier lifetime of graded-index separate-

confinement heterojunction structure is shorter than the SCH structure. This is because of the reservoir effect in the SCH structure. With suitable design of the confine-

and N_2 is also determined by the round-trip-gain requirement of the lateral modes.

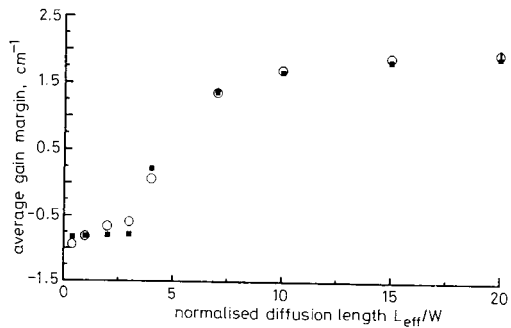


Fig. 8 Variation of average gain margin against the normalised diffusion length for $\lambda/4$ phase-shifted and uniform-grating DFB laser

■ uniform grating
○ $\lambda/4$ grating

ment structure of QW material, the gain margin between the fundamental and first-order mode can be enhanced. This improvement can be utilised to suppress lateral modes in high-power devices without reduction of the active-region width or the maximum output power.

In conclusion, we have developed a large-signal dynamic DFB-laser model with lateral modes taken into consideration. Using this model, the static and dynamic behaviour of BH DFB lasers are studied. It is found that lateral modes have a significant effect on the static and dynamic behaviour of DFB laser

(a) the gain margin between the lateral modes varies with the carrier diffusion length

(b) the excitation or suppression of the overshoot of the lateral modes is also affected by the carrier-diffusion length

(c) the lateral and longitudinal distributions of carriers are closely coupled together, and the distribution of N_1

7 References

- SIN, Y., HORIKAWA, H., and KAMIJOH, T.: 'InGaAs-GaAs-InGaP distributed feedback buried heterostructure strained quantum-well lasers for high power operation at 0.98 μm ', *IEEE Photon. Technol. Lett.*, 1993, 5, (9), pp. 966-968
- MAJOR, J., O'BRIEN, S., GULGAZOV, V., WELCH, D., and LANG, R.: 'High power singlemode AlGaAs distributed bragg reflector laser diodes operating at 856 nm', *Electron. Lett.*, 1993, 30, pp. 496-497
- KOREN, U., KOCH, T., CORVINI, P., MILLER, B., ELSENSTEIN, G., TUCKER, R., SU, Y., and CAPLK, R.: 'High-power, high-speed 1.3 μm semi-insulating-blocked distributed-feedback lasers', *J. Appl. Phys.*, 1988, 64, (9), pp. 4785-4787
- GARBUZOV, D., ANTONISHKIS, N., ZHIGULIN, N., I'IGULIN, N., KOCHERGIN, A., LIFSHTIZ, D., RAFAILOV, E., and FUKSMAN, M.: 'High-power buried InGaAsP/GaAs ($\lambda = 0.8 \mu\text{m}$) laser diodes', *Appl. Phys. Lett.*, 1993, 63, (10), pp. 1062-1064
- CHAND, N., DUTTA, N., CHU, S., SYRBU, A., MERUTZA, A., and YAKOVIEV, V.: 'High performance strained InGaAs/AlGaAs buried-heterostructure quantum-well lasers fabricated by in situ etching and regrowth', *Appl. Phys. Lett.*, 1993, 62, (15), pp. 1818-1820
- TAKAHASHI, N.S., FUKUSHIMA, A., SASAKI, T., and ISHIKAWA, J.: 'Fabrication methods for InGaAsP/GaAs visible laser structure with AlGaAs burying layers grown by liquid-phase epitaxy', *J. Appl. Phys.*, 1986, 59, (10), pp. 761-768
- YU, S., PLUMB, R., ZHANG, L., NOWELL, M., and CARROLL, J.: 'Large signal dynamic behaviour of distributed feedback lasers including lateral effects', *IEEE J. Quantum Electron.*, 1994, 30, pp. 1740-1750
- TURLEY, S.: 'Optical waveguiding in (In, Ga)(As, P) in inverted ridge waveguide lasers at 1.3 μm waveguide', *IEEE J. Quantum Electron.*, 1983, 19, (7), pp. 1186-1195
- TUCKER, R., and POPE, D.J.: 'Circuit modelling of diffusion on damping in a narrow-stripe semiconductor laser', *IEEE J. Quantum Electron.*, 1983, 19, pp. 1179-1183
- ZHANG, L., and CARROLL, J.: 'Large signal dynamic model of the DFB laser', *IEEE J. Quantum Electron.*, 1992, 28, (3), pp. 604-611
- YARIV, A.: 'Quantum electronics' (John Wiley & Sons, 1987), 3rd ed., chap. 3
- GARRETT, B., and WHITEAWAY, J.E.A.: 'Self stabilisation of the fundamental lateral mode in index-guided semiconductor lasers', *IEE Proc. J.*, 1987, 134, (1), pp. 11-15